

Voltage to Calcium Transformation Improves Direction Selectivity in *Drosophila* T4 neurons

Firstname Middlename Surname^{1,2*}, Firstname Middlename Familyname^{1,2†§},
Firstname Initials Surname^{2†¶}, Firstname Surname^{2*}

*For correspondence:

email1@example.com (FMS);
email2@example.com (FS)

[†]These authors contributed equally to this work

[‡]These authors also contributed equally to this work

Present address: [§]Department, Institute, Country; [¶]Department, Institute, Country

¹Max Planck Institute for Biological Intelligence (in foundation), Martinsried, Germany;

²Graduate School of Systemic Neurosciences, LMU Munich, Martinsried, Germany

Abstract A critical step in neural information processing is the transformation of membrane voltage into calcium signals leading to transmitter release. However, the effect of voltage to calcium transformation on neural responses to different sensory stimuli is not well understood. Here, we use in vivo two-photon imaging of genetically encoded voltage and calcium indicators, ArcLight and GCaMP6f respectively, to measure responses in *Drosophila* direction-selective T4 neurons. Comparison between ArcLight and GCaMP6f signals revealed calcium signals to have a much higher direction selectivity compared to voltage signals. Using these recordings we build a model which transforms T4 voltage responses to calcium responses. The model reproduces experimentally measured calcium responses across different visual stimuli using different temporal filtering steps and a stationary non-linearity. These findings provide a mechanistic underpinning of the voltage-to-calcium transformation and show how this processing step, in addition to synaptic mechanisms on the dendrites of T4 cells, improves direction selectivity in the output signal of T4 neurons.

Introduction

In order to guide animal behavior, neurons perform a wide range of computations. Neurons encode information via graded changes in membrane potential or action potential frequency. Mostly they communicate via chemical synapses which requires the release of neurotransmitters. When the presynaptic membrane is sufficiently depolarized, voltage-gated calcium channels open and allow Ca^{2+} to enter the cell (Luo 2020). Calcium entry leads to the fusion of synaptic vesicles with the membrane and release of neurotransmitter molecules into the synaptic cleft (Chapman 2002). As neurotransmitters diffuse across the synaptic cleft, they bind to receptors in the postsynaptic membrane, causing postsynaptic neuron to depolarize or hyperpolarize, passing the information from pre to postsynaptic neurons (Di Maio 2008). Voltage to calcium transformation in neurons is therefore a crucial step in neural information processing and neural computation.

A classic example of neural computation is how *Drosophila* neurons compute the direction of visual motion (Borst *et al.* 2020). In *Drosophila*, visual information is processed in parallel ON (contrast increments) and OFF (contrast decrements) pathways (Joesch *et al.* 2010; Eichner *et al.* 2011). Direction selectivity emerges three synapses downstream of photoreceptors, in T4 and T5 for ON and OFF pathways respectively. Four subtypes of T4 and T5 cells exist, each responding selectively to one of the four cardinal directions (Maisak *et al.* 2013). Amazingly, right at the first stage where direction selectivity emerges, T4 and T5 cells exhibit a high degree of direction selectivity,

with no responses to null direction stimuli. This statement is, however, based on calcium recordings. Whole-cell patch clamp recordings show a somewhat different picture: While preferred direction stimuli also lead to large membrane depolarizations, edges or gratings moving along the null directions elicit smaller but significant responses as well (Groschner *et al.* 2022). This hints to an additional processing step where voltage signals are transformed into calcium signals that increases direction selectivity of the cells. In order to study this step systematically, we recorded both voltage and calcium signals in response to a large stimulus set that includes gratings and edges moving along various directions at different speeds and contrasts. Using these data, we build a model that captures the transformation from voltage to calcium by a few linear and non-linear processing steps.

Results

We first expressed the genetically encoded calcium indicator GCaMP6f (Chen *et al.* 2013) in T4 cells projecting to layer 3 of the lobula plate. These cells have upward motion as their preferred direction (PD) and downward motion as their null direction (ND). We also expressed the genetically encoded voltage indicator Arclight (Jin *et al.* 2012) using the same driver line. Arclight's fluorescence decreases with membrane depolarization and increases with membrane hyperpolarization. To compare the voltage and calcium signals, we recorded the neural activity in T4c cells dendrites in medulla layer 10 in response to the same set of stimuli using 2-photon microscopy (Denk *et al.* 1990). The complete stimuli set included square-wave gratings of 30° spatial wavelength moving in 12 different directions, and ON edge moving in PD and ND, at four different speeds ($15^\circ s^{-1}$, $30^\circ s^{-1}$, $60^\circ s^{-1}$, $90^\circ s^{-1}$) and four different contrasts (10%, 20%, 50%, 100%).

In a first set of experiments, we measured the voltage and calcium signals in response to gratings moving in PD and ND at four different speeds (figure 1A). As the grating stimuli consists of alternate bright and dark bars moving in a certain direction, there was a modulation in the Arclight (black traces) and GCaMP6f (red traces) responses to it. The GCaMP6f responses showed modulations only for slower speeds, while Arclight responses had modulations also for faster speeds. The response amplitudes were much higher for GCaMP6f ($\approx 2.0\Delta F/F$) compared to Arclight ($\approx -0.06\Delta F/F$). The peak responses (maximum $\Delta F/F$) decreased with increasing stimulus speed both for GCaMP6f and Arclight (figure 1B). To understand if voltage to calcium transformation affects direction selectivity in T4 cells, we compared the responses to gratings moving in PD and ND. GCaMP6f responses in ND were negligible compared to its responses in PD, while for Arclight responses in ND were quite visible compared to responses in PD. We quantified the direction selectivity using a direction selectivity index (DSI) calculated as the difference of the peak responses to preferred and null direction, divided by the sum of the peak responses (Materials and Methods equation (1)). The results revealed a high degree of direction selectivity of ≈ 0.8 for GCaMP6f at slower velocities, compared to a direction selectivity of ≈ 0.4 for Arclight (figure 1E). For both GCaMP6f and Arclight signals, direction selectivity decreased with increasing velocity.

Next, instead of gratings, we used a moving bright edge with all other stimulus parameters remaining the same (figure 1C). As the edge moves upward on the screen, it crosses the receptive field of T4c neurons ($\approx 15^\circ$) only once. Hence, there was only a single peak in the response. The peak response decreased with increasing stimulus speed for GCaMP6f, while the peak response remained almost constant for Arclight throughout all speeds (figure 1D). When comparing edge responses moving along preferred and null directions, GCaMP6f showed negligible responses in null direction while Arclight revealed considerable responses to null direction stimuli. The direction selectivity index was again much higher for GCaMP6f compared to Arclight (figure 1F). Together these results show that GCaMP6f signals have a high level of direction selectivity compared to Arclight signals, both for grating and edge stimuli.

The stimulus strength was further varied by changing the contrast between bright and dark bars for gratings and between moving edge and background for edge stimuli. We measured Arclight and GCaMP6f responses to gratings moving at $30^\circ s^{-1}$ at four different contrasts (figure 2A). Increasing

91 contrast increases stimulus strength, resulting in an increase in response for both Arclight and
92 GCaMP6f. GCaMP6f signals were modulated at the temporal frequency of the grating but showed
93 an additional rise over time. This slow increase was not observed in Arclight signals. We also
94 measured Arclight and GCaMP6f responses to ON edges moving at the same speed but having
95 different contrasts (figure 2C). The peak response (maximum $\Delta F/F$) increased with increasing
96 contrast (figure 2D). Similar to previous experiments, the direction selectivity index was much higher
97 for GCaMP6f (≈ 0.9) compared to that for Arclight (≈ 0.4) (figure 2E,F).

98 In the results presented so far we compared responses for two directions only, i.e. along
99 the preferred (upward) and along the null direction (downward). We next wanted to extend the
100 comparison to motion along 12 directions, from 0° to 360° in steps of 30° . For this comparison, we
101 determined the normalized peak responses of Arclight and GCaMP6f signals to gratings moving
102 in 12 directions at 4 different speeds and 4 different contrasts, respectively (figure 3A, B). The
103 directional tuning was much sharper for GCaMP6f compared to Arclight. To quantify this we
104 calculated the directional tuning index L_{dir} (Mazurek *et al.* 2014) for each speed and each contrast
105 as the vector sum of the peak responses divided by the sum of all individual vector magnitudes
106 (Materials and Methods equation (2)). In general, the directional tuning indices again were much
107 higher for GCaMP6f (≈ 0.7) compared to that of Arclight (≈ 0.2) (figure 3C, D). These results together
108 show that GCaMP6f signals have a higher degree of directional tuning across different speeds and
109 contrasts than Arclight.

110 How does the voltage to calcium transformation lead to calcium signals with significantly higher
111 directional tuning compared to voltage signals? To address this question, we constructed an
112 algorithmic model (figure 4) which takes Arclight signals as inputs and outputs GCaMP signal. In
113 order to find the optimal parameter values, we first defined an error function. For each stimulus
114 condition, the error was calculated as the sum of the squared difference between the model and
115 experimental data at each time-point (Materials and Methods equation (3)). There were a total
116 of 112 stimulus conditions: gratings speed (48), gratings contrast (48), edge speed (8) and edge
117 contrast (8). Thus, the total error amounted to the sum of errors across all stimulus conditions
118 (Materials and Methods equation (4)). We then found the optimal parameters values of the model
119 that correspond to the minimum total error using Python SciPy optimize minimize function (Virtanen
120 *et al.* 2020).

121 We started with a simple model (figure 4A). The model first passes the Arclight signal through
122 a high-pass filter. The high-pass filter brings the input Arclight signal closer to the actual voltage
123 signal by removing the slowly fluctuating Arclight indicator dynamics. This is followed by a threshold,
124 assuming that the voltage changes below a certain threshold does not affect the calcium level in
125 the cell. Now, few experimental observations which we took into consideration for building up the
126 model further were as follows : First, the GCaMP6f response to gratings showed modulations only
127 for slower speeds, whereas Arclight response had modulations even at faster speeds (figure 1A).
128 This suggests that the GCaMP6f signal is a low-pass filtered version of the Arclight signal. In the
129 simple model, we used a single low-pass filter followed by a gain and time-shift. Multiplication with
130 a gain factor was required since GCaMP6f signals have a much higher magnitude compared to
131 Arclight. Arclight and GCaMP6f responses were recorded from cells in different flies with different
132 receptive fields, therefore the responses can have different phases, and a time-shift is necessary
133 to align the signals. However, the simple model with single low-pass filter could not reproduce
134 responses across all stimuli. To compare the model performances, we defined a model error as
135 the total error divided by the power of the data (Materials and Methods equation (5)). The model
136 error for the complete dataset fit for the simple model was around 34%. Specifically, the simple
137 model failed to reproduce the edge responses. Second, the GCaMP6f responses in addition to
138 modulation also had a steady rise over time whereas Arclight signal only had modulations (figure 1A,
139 2A). For reproducing the edge responses and modulation in grating responses, the model needed
140 a low-pass filter with a small time constant. However to simulate the steady rise in the grating
141 signal, a low-pass filter with a large time constant was necessary. Hence, we combined the output

of two low-pass filters. Summing up the low-pass filter outputs (figure 4B) did not lead to much improvement. However, combining both outputs from the low-pass filters with a multiplication led to significant decrease in the error. The model error for the multiplicative model (figure 4C) then was around 20%.

The multiplicative model thus has in total 6 parameters - high-pass filter time constant, threshold, low-pass filter 1 time constant, low-pass filter 2 time constant, gain and shift. The multiplicative model was able to reproduce calcium signals across different visual stimuli (figure 5). It could reproduce both the modulation as well as slow rise in the GCaMP6f signal in response to gratings (figure 5A). The model could also reproduce the ON edge speed tuning responses across different speeds (figure 5C,D). The directional tuning index L_{dir} were similar for model and experimental data across slower speeds and all contrasts (figure 5E,F). Thus the model was able to successfully reproduce experimental calcium data across different stimuli.

Is the slow rise in GCaMP6f signals over time due to the properties of T4 cells or due to the properties of GCaMP6f? To answer this question we used a faster version of the calcium indicator GCaMP8f (Zhang *et al.* 2020). GCaMP8f was expressed in T4c cells using the same driver line. The experiments were repeated using grating stimuli in 12 directions at 4 speeds and ON edges moving in PD and ND. T4c cells GCaMP8f responses were similar to GCaMP6f responses but faster. As with GCaMP6f, GCaMP8f signals had modulation and slow rise over time. We further compared the model parameters values for GCaMP6f data fit and GCaMP8f data fit (figure 6). The model parameters were similar with time constants having smaller values for GCaMP8f as it is a faster indicator. Therefore, the slow rise in the calcium signal is not due to the properties of GCaMP6f indicator.

While the T4 cells' Arclight responses to gratings show only modulation, their GCaMP responses show modulation and slow increases over time. Does this response occur exclusively in direction-selective T4 cells or does it also occur in non-direction-selective cells? In order to answer this question, we expressed Arclight & GCaMP6f in medulla neurons Mi1 & Tm3 cells, which are both non-direction-selective. Mi1 and Tm3 are pre-synaptic to T4 cells and have ON-center receptive field (Behnia *et al.* 2014; Arenz *et al.* 2017). We measured Mi1, Tm3 Arclight (black) and GCaMP6f (red) responses to gratings moving at 4 different speeds and to gratings moving at 4 different contrasts (figure 7). The gratings were moved in only one direction, since the direction does not affect non-direction-selective cells' responses. Contrary to T4, Mi1 GCaMP6f responses had only modulation without a slow increase over time (figure 7A). Tm3 GCaMP responses did not increase over time, and showed only modulation for gratings moving at $15^\circ s^{-1}$. For gratings moving at $30^\circ s^{-1}$ and $60^\circ s^{-1}$, there was an increase in Tm3 GCaMP6f response over time, but the Arclight response also already had a slow increment over time (figure 7A). Similar to T4, the peak response for Mi1 and Tm3 decreased with an increase in speed and increased with an increase in contrast (figure 7B, D). Together, these results show that voltage to calcium transformation causes GCaMP6f response increment over time only for direction-selective T4 cells and not for non-direction-selective Mi1 and Tm3 cells.

Next, we used the model described in figure 4 to reproduce Mi1 and Tm3 calcium responses using their Arclight responses. As discussed earlier, the simple model (figure 4A) with single low-pass filter was not able to reproduce T4 calcium responses across all stimuli. However, for Mi1 and Tm3, the simple model with a single low-pass filter was able to reproduce the calcium responses across all stimuli conditions (figure 8). The model also accurately replicated the speed and contrast tuning for Mi1 and Tm3 (figure 8B, D). We further compared the model error for simple and multiplicative model for Mi1, Tm3 and T4c data (figure 9). The model error for Mi1 and Tm3 for simple model was $\approx 6.5\%$ and $\approx 5.9\%$ respectively compared to $\approx 11.9\%$ and $\approx 7\%$ for the multiplicative model. Thus, the simple model already performed well for Mi1 and Tm3 dataset, and changing to multiplicative model did not improve the performance. For the T4c dataset the model error was $\approx 34\%$ and $\approx 21\%$ for the simple and multiplicative model respectively. Hence, the multiplicative model with two low-pass filters performed better for T4c dataset whereas for Mi1 and

193 Tm3 the Simple model with single low-pass filter was sufficient to reproduce the calcium responses.
194 This suggests that voltage-to-calcium transformation is more complex for direction-selective cell T4
195 than for the non-direction-selective cells Mi1 and Tm3.

196 Discussion

197 Neuronal signaling and information processing involves the transformation of membrane voltage
198 into calcium signals, which lead to transmitter release. Computations can occur at different stages
199 in the signal chain: 1.) dendritic integration and processing of voltage signals. 2.) the transformation
200 from voltage to calcium and 3.) between calcium and neurotransmitter release. In this study, we
201 explored the transformation of voltage to calcium in T4-cells. T4 neurons are the first direction-
202 selective neurons in the *Drosophila* ON motion vision pathway.

203 We found that the voltage to calcium transformation in T4c neurons improves direction selectiv-
204 ity, and calcium signals in T4c cells have a much higher direction selectivity and tuning compared to
205 membrane voltage across different stimuli conditions (figure 1-3). The direction selectivity index for
206 calcium signals compared with voltage signals was also much higher in a voltage imaging study in
207 T5 cells using ASAP2f (Wienecke *et al.* 2018). As calcium is required for neurotransmitter release, this
208 would increase the direction selectivity of T4/T5 cells' output signals. In the lobula plate, T4/T5 cells
209 provide inputs onto large lobula plate tangential cells (LPTCs) that are depolarized during preferred
210 and hyperpolarized during null direction motion (Maus, Meier, *et al.* 2014). For example, vertical
211 system (VS) cells with dendrites in layer 4 receive direct excitatory inputs from downward tuned
212 T4d/T5d neurons causing depolarization during motion in the downward preferred direction. These
213 VS cells also receive indirect inhibitory inputs from upward tuned T4c/T5c neurons via glutamatergic
214 LPI3-4 neurons projecting from layer 3 to layer 4 causing hyperpolarization in VS cells during motion
215 in the upward null direction. Upon silencing LPI3-4 neurons' synaptic output via tetanus toxin, VS
216 neurons depolarization response in the preferred direction did not change, but the null direction
217 response was almost absent (Maus, Pankova, *et al.* 2015). This suggests that T4/T5 output is nearly
218 perfectly tuned and there is no output response in the null direction, which is similar to our findings
219 for the calcium responses. Thus, voltage to calcium transformation increases direction selectivity in
220 T4/T5 cells and this enhances direction selectivity in signals further downstream.

221 Electrophysiology has been the most frequently used method to measure the membrane po-
222 tential changes in neurons. However, due to the small size of neurons in the optic lobe, single-cell
223 electrophysiological recordings of these neurons have been difficult. Genetically encoded voltage
224 indicators (GEVIs) have evolved as powerful tools for recording changes in neuronal membrane
225 potentials. Optical methods of monitoring brain activity are appealing because they allow simul-
226 taneous, noninvasive monitoring of activity in many individual neurons. We used a fluorescence
227 protein (FP) voltage sensor called ArcLight (Jin *et al.* 2012). ArcLight is based on the fusion of the
228 voltage-sensing domain of *Ciona intestinalis* voltage-sensitive phosphatase (Murata *et al.* 2005) and
229 the fluorescent protein super ecliptic pHluorin with an A227D mutation. ArcLight has been shown to
230 robustly report both subthreshold events and action potentials in genetically targeted neurons in
231 the intact *Drosophila* brain (Cao *et al.* 2013).

232 We built a model to capture voltage to calcium transformation in T4c, Mi1, and Tm3 cells. A
233 simple model with a single low-pass filter was able to reproduce calcium responses in non-direction-
234 selective Mi1 and Tm3 cells (figure 8), whereas a more complex model combining the output of
235 two low-pass filters via a multiplication was required to reproduce T4c calcium responses (figure 5).
236 This suggests that voltage-calcium transformation in Mi1 and Tm3 cells is different from those in
237 T4c cells. The direction selectivity for the simple model signals for T4c was much lower compared
238 to the multiplicative model. The time constants for the two low-pass filters were identical for the
239 multiplicative model for T4c data fit. Thus, these two low-pass filters in the multiplicative model
240 could also be replaced by a single low-pass filter followed by a quadratic non-linearity. An exponent
241 of close to 2 (exact value: 2.2) was found in the parameter search for a model with a single low-pass
242 filter followed by an exponential nonlinearity.

Differential expression of voltage-gated calcium channels in these cells could explain the different voltage to calcium transformation. Voltage-gated calcium channels mediate depolarization-induced calcium influx that drives the release of neurotransmitters. The $\alpha 1$ -subunit of the voltage-gated calcium channels forms the ion-conducting pore, which makes it distinct from other calcium channels. Three families of genes encode $\alpha 1$ subunits. *Drosophila* genome has one $\alpha 1$ subunit gene in each family: $\alpha 1D$ (Ca_v1), cac (Ca_v2), and $\alpha 1T$ (Ca_v3) (Littleton & Ganetzky 2000; King 2007). In *Drosophila* antennal lobe projection neurons, cac (Ca_v2) type and $\alpha 1T$ (Ca_v3) type voltage-gated calcium channels are involved in sustained and transient calcium currents, respectively (Gu *et al.* 2009; Iniguez *et al.* 2013). According to a RNA-sequencing study (Davis *et al.* 2020), $\alpha 1T$ (Ca_v3) mRNA have higher expression in Mi1 (2050.16 Transcripts per Million (TPM)) compared to T4 (686.68 TPM) and Tm3 (336.45 TPM). While cac (Ca_v2) mRNA have higher expression in T4 (1298.53 TPM) compared to Mi1 (986.25 TPM) and Tm3 (817.61 TPM). Different expression of voltage-gated calcium channels could cause different voltage to calcium transformations in non-direction selective and direction-selective cells.

Materials and Methods

Flies

Flies (*Drosophila melanogaster*) were raised at 25°C and 60% humidity on a 12 hour light/12 hour dark cycle on standard cornmeal agar medium. For calcium imaging experiments, genetically-encoded calcium indicator GCaMP6f (Chen *et al.* 2013) was expressed in T4 neurons with axon terminals predominantly in layer 3 of the lobula plate. Similarly for voltage imaging experiments, genetically-encoded voltage indicator Arclight (Jin *et al.* 2012) was expressed in T4 layer 3 neurons. The flies genotype were as follows :

1. T4c>GCaMP6f : w+ ; VT15785-Gal4AD / UAS-GCaMP6f; VT50384-Gal4DBD / UAS-GCaMP6f
2. T4c>Arclight : w+ ; VT15785-Gal4AD / UAS-Arclight; VT50384-Gal4DBD / +

For Mi1 and Tm3 experiments, the flies genotype were as follows :

1. Mi1>GCaMP6f : w+ ; R19F01-Gal4AD / UAS-GCaMP6f; R71D01-Gal4DBD / UAS-GCaMP6f
2. Mi1>Arclight : w+ ; R19F01-Gal4AD / UAS-Arclight; R71D01-Gal4DBD / +
3. Tm3>GCaMP6f : w+ ; R13E12-Gal4AD / UAS-GCaMP6f; R59C10-Gal4DBD / UAS-GCaMP6f
4. Tm3>Arclight : w+ ; R13E12-Gal4AD / UAS-Arclight; R59C10-Gal4DBD / +

Calcium & voltage imaging

For imaging experiments, fly surgeries were performed as previously described (Maisak *et al.* 2013). Briefly, flies were anaesthetized with CO₂ or on ice, fixed with their backs, legs and wings to a Plexiglas holder with back of the head exposed to a recording chamber filled with fly external solution. The cuticula at the back of the head on one side of the brain was cut away with a fine hypodermic needle and removed together with air sacks covering the underlying optic lobe. The neuronal activity was then measured from optic lobe on a custom-built 2-photon microscope as previously described (Maisak *et al.* 2013). Images were acquired at 64 x 64 pixels resolution and frame rate 13 Hz with the Scanimage software in Matlab (Pologruto *et al.* 2003).

Visual stimulation

For the study of visual responses of T4c cells, visual stimuli were presented on a custom-built projector-based arena as described in (Arenz *et al.* 2017). In brief : Two micro-projectors (TI DLP Lightcrafter 3000) were used to project stimuli onto the back of an opaque cylindrical screen covering 180° in azimuth and 105° in elevation of the fly's visual field. To increase the refresh rate from 60 Hz to 180 Hz (at 8 bit color depth), projectors were programmed to use only green LED (OSRAM L CG H9RN) which emits light between 500 nm to 600 nm wavelength. Two long-pass filters (Thorlabs FEL0550 and FGL550) were placed in front of each projector to restrict the stimulus light

to wavelengths above 550 nm. This prevents overlap between GCaMP signal and arena light spectra. To allow only GCaMP emission spectrum to be detected, a band-pass filter (Brightline 520/35) was placed in-front of the photomultiplier. For all stimuli used here, we set the medium brightness to a 8-bit grayscale value of 50, which corresponds to a medium luminance of $55 \pm 11 \text{ cd/m}^2$. Stimuli were rendered using custom written software in Python 2.7.

Stimuli

Stimuli were presented with 3-5 repetitions per experiment in a randomized fashion. To measure the directional and speed tuning, square-wave gratings with a spatial wavelength of 30° spanning the full extent of the stimulus arena were used. The gratings were moved in 12 different directions from $0^\circ - 360^\circ$ at 4 different speeds (15° s^{-1} , 30° s^{-1} , 60° s^{-1} , 120° s^{-1}). Similarly, to measure direction and contrast tuning, square-wave gratings with a spatial wavelength of 30° spanning the full extent of the stimulus arena were used. The gratings moved at a speed of 30° s^{-1} in 12 different directions at 4 different contrasts (10%, 20%, 50%, 100%). Edge responses were measured using ON edge i.e. bright edge moving on a dark background with full contrast. The ON edge moved in preferred direction (upward) or null direction (downward) at 4 different speeds (15° s^{-1} , 30° s^{-1} , 60° s^{-1} , 120° s^{-1}).

Data analysis

Data analysis was performed using custom-written routines in Matlab and Python 2.7, 3.7. Images were automatically registered using horizontal and vertical translations to correct for the movement of brain. Fluorescence changes ($\Delta F/F$) were then calculated using a standard baseline algorithm (Jia *et al.* 2011). Regions of interest (ROIs) were drawn on the average raw image manually by hand in the medulla layer M10 for signals from T4 dendrites. Averaging the fluorescence change over this ROI in space resulted in a ($\Delta F/F$) time course. Voltage imaging with Arclight and calcium imaging with GCaMP6f and GCaMP8f were performed and analysed using same settings.

The direction selectivity was evaluated using a direction selectivity index (DSI) calculated as the difference of the peak responses to preferred and null direction, divided by the sum of the peak responses:

$$DSI = \frac{PD_{peak} - ND_{peak}}{PD_{peak} + ND_{peak}} \quad (1)$$

In the above measurement, only the difference in response between the two opposing directions of motion is quantified. To take into account all 12 directions of motion, we calculated the directional tuning index:

$$L_{dir} = \left| \frac{\sum_{\varphi} \vec{v}(\varphi)}{\sum_{\varphi} |\vec{v}(\varphi)|} \right| \quad (2)$$

where $\vec{v}(\varphi)$ is a vector proportionally scaled with the mean response and points in the direction corresponding to the direction of motion given by the rotation angle φ of the stimulus (Mazurek *et al.* 2014).

Model simulations

Custom-written Python3.7 scripts were used to simulate the models (figure 4). To calculate the optimal parameter values, we first defined an error function. For each stimulus condition (s_i), the error was calculated as:

$$error(s_i) = \sum_{t=0}^{t=N} (model(s_i t) - data(s_i t))^2 \quad (3)$$

The model took as input Arclight data across all 112 different stimuli conditions. Next, we summed the error for all stimuli conditions:

$$total\ error = \sum_{i=1}^{i=112} error(s_i) \quad (4)$$

327 The model parameters were first assigned a random value within the defined parameter bounds.
 328 Python SciPy optimize minimize function then used the L-BFGS-B (Limited Broyden Fletcher Goldfarb
 329 Shanno) algorithm to find the parameter values corresponding to the minimum total error. A total
 330 of 300 runs were performed, and the parameter values that corresponded to the run with the
 331 lowest error were used to produce the final output signals. To compare the model performances,
 332 we calculated the model error as:

$$\text{model error [\% of data power]} = \frac{\text{total error}}{\sum_{i=1}^{112} (\text{data}(s_i))^2} \quad (5)$$

333 References

- 334 1. Denk, W., Strickler, J. H. & Webb, W. W. Two-photon laser scanning fluorescence microscopy.
 335 *Science* **248**, 73–76 (1990). doi: [10.1126/science.2321027](https://doi.org/10.1126/science.2321027)
- 336 2. Littleton, J. T. & Ganetzky, B. Ion channels and synaptic organization: analysis of the *Drosophila*
 337 genome. *Neuron* **26**, 35–43 (2000). doi: [10.1016/s0896-6273\(00\)81135-6](https://doi.org/10.1016/s0896-6273(00)81135-6)
- 338 3. Chapman, E. R. Synaptotagmin: a Ca²⁺ sensor that triggers exocytosis? *Nature Reviews Molecu-*
 339 *lar Cell Biology* **3**, 498–508 (2002). doi: [10.1038/nrm855](https://doi.org/10.1038/nrm855)
- 340 4. Pologruto, T. A., Sabatini, B. L. & Svoboda, K. ScanImage: flexible software for operating laser
 341 scanning microscopes. *Biomedical engineering online* **2**, 1–9 (2003). doi: [10.1186/1475-925X-2-13](https://doi.org/10.1186/1475-925X-2-13)
- 342 5. Murata, Y., Iwasaki, H., Sasaki, M., Inaba, K. & Okamura, Y. Phosphoinositide phosphatase
 343 activity coupled to an intrinsic voltage sensor. *Nature* **435**, 1239–1243 (2005). doi: [10.1038/nature03650](https://doi.org/10.1038/nature03650)
- 344 6. King, G. F. Modulation of insect CaV channels by peptidic spider toxins. *Toxicon* **49**, 513–530
 345 (2007). doi: [10.1016/j.toxicon.2006.11.012](https://doi.org/10.1016/j.toxicon.2006.11.012)
- 346 7. Di Maio, V. Regulation of information passing by synaptic transmission: a short review. *Brain*
 347 *research* **1225**, 26–38 (2008). doi: [10.1016/j.brainres.2008.06.016](https://doi.org/10.1016/j.brainres.2008.06.016)
- 348 8. Gu, H. *et al.* Cav2-type calcium channels encoded by cac regulate AP-independent neurotrans-
 349 mitter release at cholinergic synapses in adult *Drosophila* brain. *Journal of neurophysiology*
 350 **101**, 42–53 (2009). doi: [10.1152/jn.91103.2008](https://doi.org/10.1152/jn.91103.2008)
- 351 9. Joesch, M., Schnell, B., Raghu, S. V., Reiff, D. F. & Borst, A. ON and OFF pathways in *Drosophila*
 352 motion vision. *Nature* **468**, 300–304 (2010). doi: [10.1038/nature09545](https://doi.org/10.1038/nature09545)
- 353 10. Eichner, H., Joesch, M., Schnell, B., Reiff, D. F. & Borst, A. Internal structure of the fly elementary
 354 motion detector. *Neuron* **70**, 1155–1164 (2011). doi: [10.1016/j.neuron.2011.03.028](https://doi.org/10.1016/j.neuron.2011.03.028)
- 355 11. Jia, H., Rochefort, N. L., Chen, X. & Konnerth, A. In vivo two-photon imaging of sensory-
 356 evoked dendritic calcium signals in cortical neurons. *Nature protocols* **6**, 28–35 (2011). doi:
 357 [10.1038/nprot.2010.169](https://doi.org/10.1038/nprot.2010.169)
- 358 12. Jin, L. *et al.* Single action potentials and subthreshold electrical events imaged in neurons with a
 359 fluorescent protein voltage probe. *Neuron* **75**, 779–785 (2012). doi: [10.1016/j.neuron.2012.06.040](https://doi.org/10.1016/j.neuron.2012.06.040)
- 360 13. Cao, G. *et al.* Genetically targeted optical electrophysiology in intact neural circuits. *Cell* **154**,
 361 904–913 (2013). doi: [10.1016/j.cell.2013.07.027](https://doi.org/10.1016/j.cell.2013.07.027)
- 362 14. Chen, T.-W. *et al.* Ultrasensitive fluorescent proteins for imaging neuronal activity. *Nature* **499**,
 363 295–300 (2013). doi: [10.1038/nature12354](https://doi.org/10.1038/nature12354)
- 364 15. Iniguez, J., Schutte, S. S. & O'Dowd, D. K. Cav3-type $\alpha 1T$ calcium channels mediate transient
 365 calcium currents that regulate repetitive firing in *Drosophila* antennal lobe PNs. *Journal of*
 366 *neurophysiology* **110**, 1490–1496 (2013). doi: [10.1152/jn.00368.2013](https://doi.org/10.1152/jn.00368.2013)
- 367 16. Maisak, M. S. *et al.* A directional tuning map of *Drosophila* elementary motion detectors. *Nature*
 368 **500**, 212–216 (2013). doi: [10.1038/nature12320](https://doi.org/10.1038/nature12320)
- 369

- 370 17. Behnia, R., Clark, D. A., Carter, A. G., Clandinin, T. R. & Desplan, C. Processing properties of
371 ON and OFF pathways for *Drosophila* motion detection. *Nature* **512**, 427–430 (2014). doi:
372 [10.1038/nature13427](https://doi.org/10.1038/nature13427)
- 373 18. Mauss, A. S., Meier, M., Serbe, E. & Borst, A. Optogenetic and pharmacologic dissection of
374 feedforward inhibition in *Drosophila* motion vision. *Journal of Neuroscience* **34**, 2254–2263
375 (2014). doi: [10.1523/JNEUROSCI.3938-13.2014](https://doi.org/10.1523/JNEUROSCI.3938-13.2014)
- 376 19. Mazurek, M., Kager, M. & Van Hooser, S. D. Robust quantification of orientation selectivity and
377 direction selectivity. *Frontiers in neural circuits* **8**, 92 (2014). doi: [10.3389/fncir.2014.00092](https://doi.org/10.3389/fncir.2014.00092)
- 378 20. Mauss, A. S., Pankova, K., *et al.* Neural circuit to integrate opposing motions in the visual field.
379 *Cell* **162**, 351–362 (2015). doi: [10.1016/j.cell.2015.06.035](https://doi.org/10.1016/j.cell.2015.06.035)
- 380 21. Arenz, A., Drews, M. S., Richter, F. G., Ammer, G. & Borst, A. The temporal tuning of the
381 *Drosophila* motion detectors is determined by the dynamics of their input elements. *Current*
382 *Biology* **27**, 929–944 (2017). doi: [10.1016/j.cub.2017.01.051](https://doi.org/10.1016/j.cub.2017.01.051)
- 383 22. Wienecke, C. F., Leong, J. C. & Clandinin, T. R. Linear summation underlies direction selectivity
384 in *Drosophila*. *Neuron* **99**, 680–688 (2018). doi: [10.1016/j.neuron.2018.07.005](https://doi.org/10.1016/j.neuron.2018.07.005)
- 385 23. Borst, A., Haag, J. & Mauss, A. S. How fly neurons compute the direction of visual motion.
386 *Journal of Comparative Physiology A* **206**, 109–124 (2020). doi: [10.1007/s00359-019-01375-9](https://doi.org/10.1007/s00359-019-01375-9)
- 387 24. Davis, F. P. *et al.* A genetic, genomic, and computational resource for exploring neural circuit
388 function. *Elife* **9**, e50901 (2020). doi: [10.7554/eLife.50901](https://doi.org/10.7554/eLife.50901)
- 389 25. Luo, L. *Principles of Neurobiology* (Garland Science, 2020). doi: [10.1201/9781003053972](https://doi.org/10.1201/9781003053972)
- 390 26. Virtanen, P. *et al.* SciPy 1.0: fundamental algorithms for scientific computing in Python. *Nature*
391 *methods* **17**, 261–272 (2020). doi: [10.1038/s41592-019-0686-2](https://doi.org/10.1038/s41592-019-0686-2)
- 392 27. Zhang, Y. *et al.* jRCaMP1.0 Fast genetically encoded calcium indicators. *Online resource* (2020).
393 doi: [10.25378/janelia.13148243.v4](https://doi.org/10.25378/janelia.13148243.v4)
- 394 28. Groschner, L. N., Malis, J. G., Zuidinga, B. & Borst, A. A biophysical account of multiplication by
395 a single neuron. *Nature* **603**, 119–123 (2022). doi: [10.1038/s41586-022-04428-3](https://doi.org/10.1038/s41586-022-04428-3)

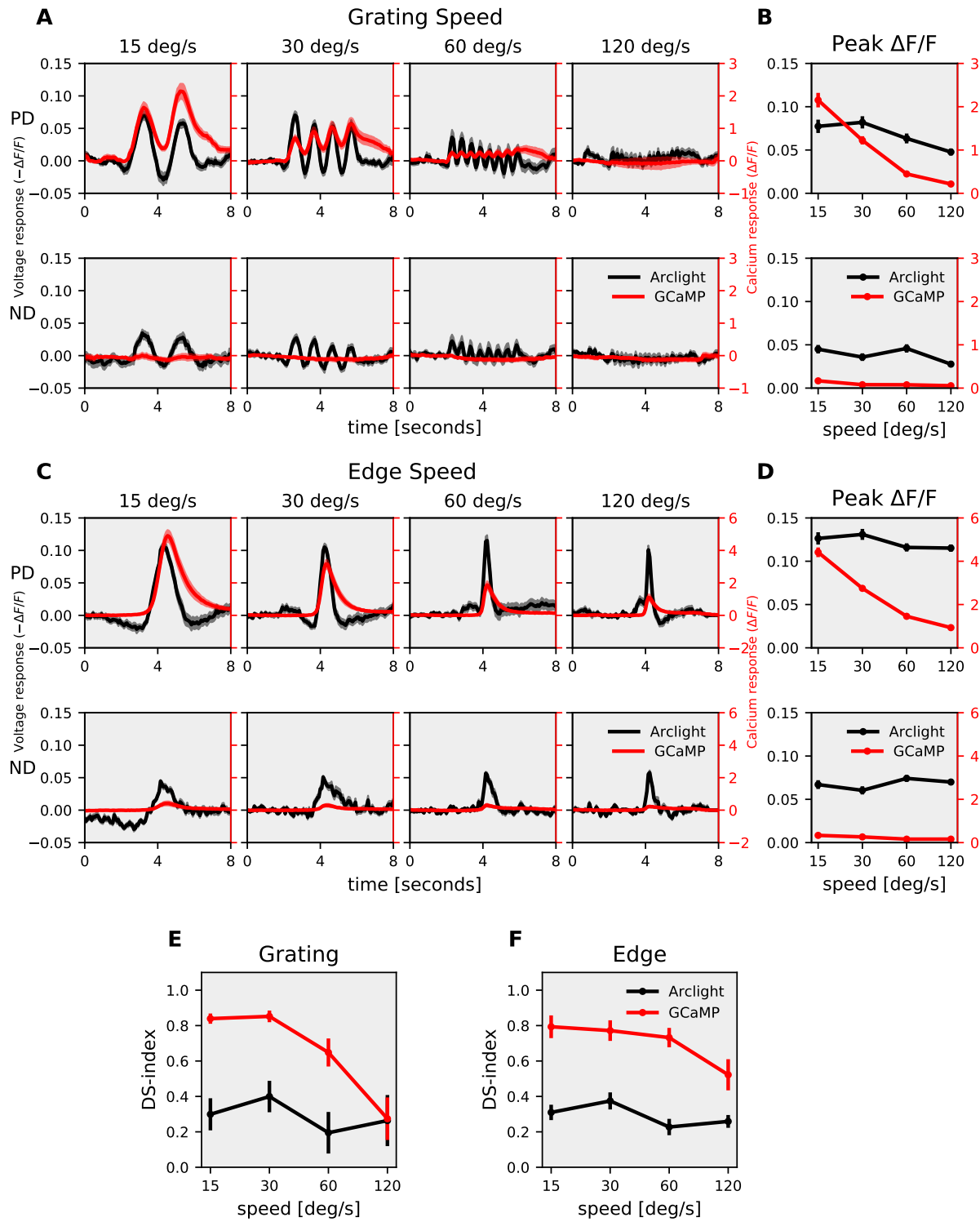


Figure 1. T4c speed dependence : (A) T4c Arclight (black) and GCaMP6f (red) responses to grating moving in PD (top row) and ND (bottom row) at 4 different speeds. The plots have twin y-axis. The left y-axis of the plot represents voltage responses i.e. changes in Arclight fluorescence ($-\Delta F/F$) and the right y-axis of the plot represents calcium responses i.e. changes in GCaMP6f fluorescence ($\Delta F/F$) (B) T4c peak responses to grating moving in PD (top) and ND (bottom) at 4 different speeds. (n = 20 ROIs from N = 10 flies for Arclight, n = 18, N = 9 for GCaMP6f) (C) T4c Arclight (black) and GCaMP6f (red) responses to ON-edge moving in PD (top row) and ND (bottom row) at 4 different speeds. (D) T4c peak responses to ON-edge moving in PD and ND at 4 different speeds. (n = 29, N = 10 for Arclight, n = 17, N = 4 for GCaMP6f) (E) Direction selectivity index (DSI) calculated as difference of peak responses in PD and ND divided by the sum of peak responses for grating. (F) Direction selectivity index (DSI) for ON-edge. All data shows the mean \pm SEM. PD: preferred direction, ND: null direction.

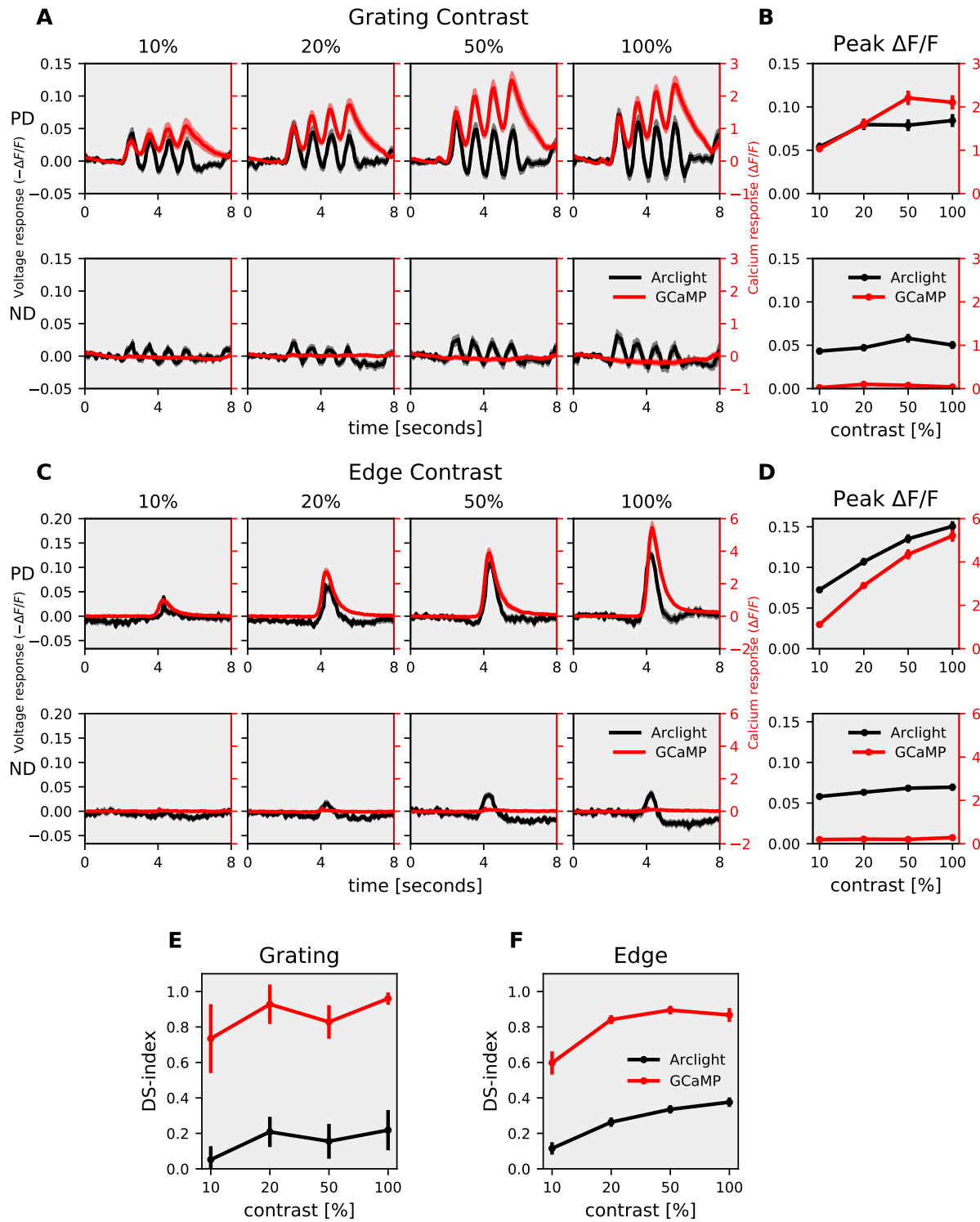


Figure 2. T4c contrast dependence : (A) T4c Arclight (black) and GCaMP6f (red) responses to grating moving in PD (top row) and ND (bottom row) at 4 different contrasts. The plots have twin y-axis. The left y-axis of the plot represents voltage responses i.e. changes in Arclight fluorescence ($-\Delta F/F$) and the right y-axis of the plot represents calcium responses i.e. changes in GCaMP6f fluorescence ($\Delta F/F$) (B) T4c peak responses to grating moving in PD (top) and ND (bottom) at 4 different contrasts. (n = 23 ROIs from N = 11 flies for Arclight, n = 22, N = 9 for GCaMP6f) (C) T4c Arclight (black) and GCaMP6f (red) responses to ON-edge moving in PD (top row) and ND (bottom row) at 4 different contrasts. (D) T4c peak responses to ON-edge moving in PD and ND at 4 different contrasts. (n = 36, N = 5 for Arclight, n = 41, N = 7 for GCaMP6f) (E) Direction selectivity index (DSI) calculated as difference of peak responses in PD and ND divided by the sum of peak responses for grating. (F) Direction Selectivity Index (DSI) for ON-edge. All data shows the mean \pm SEM.

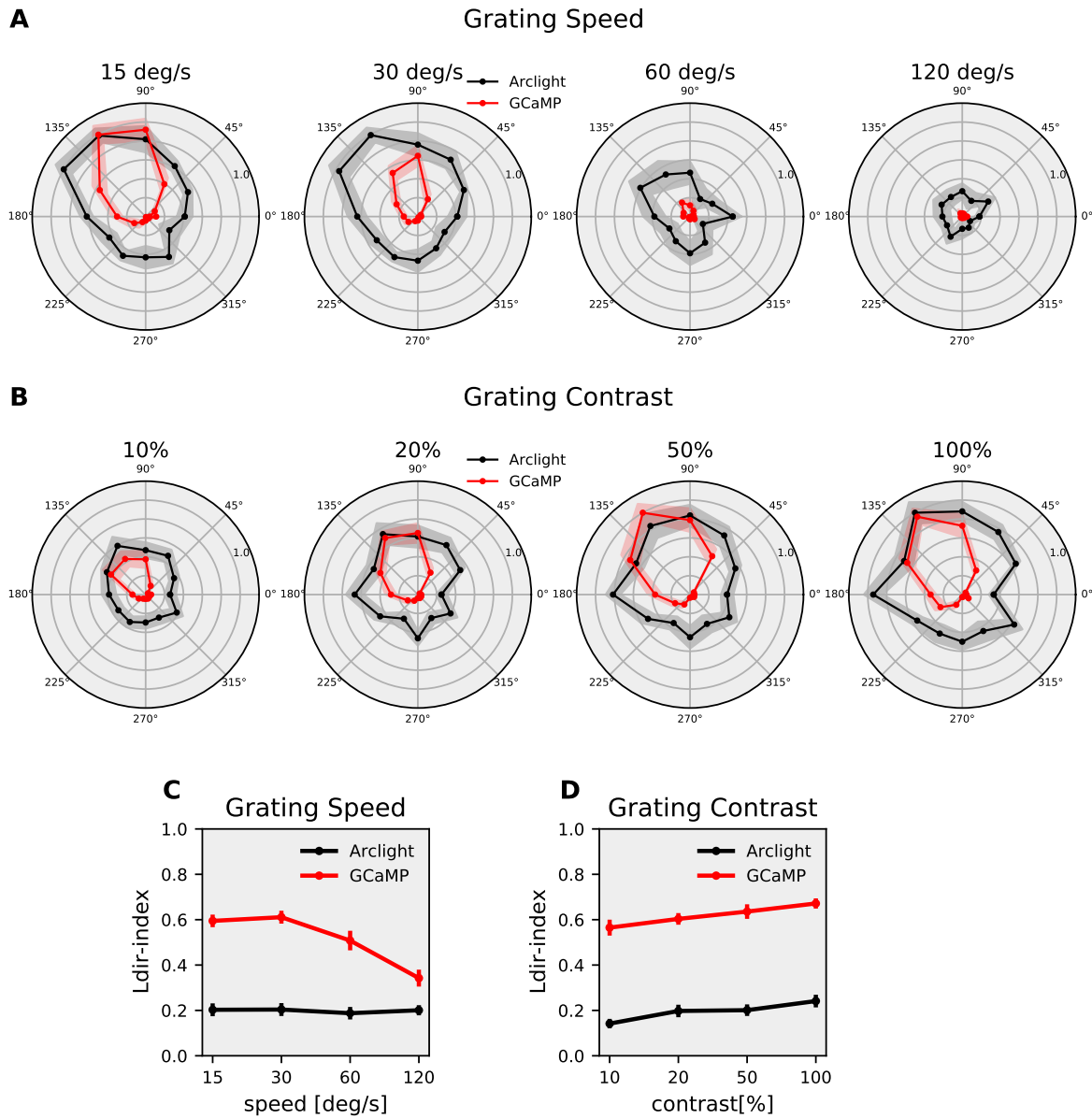
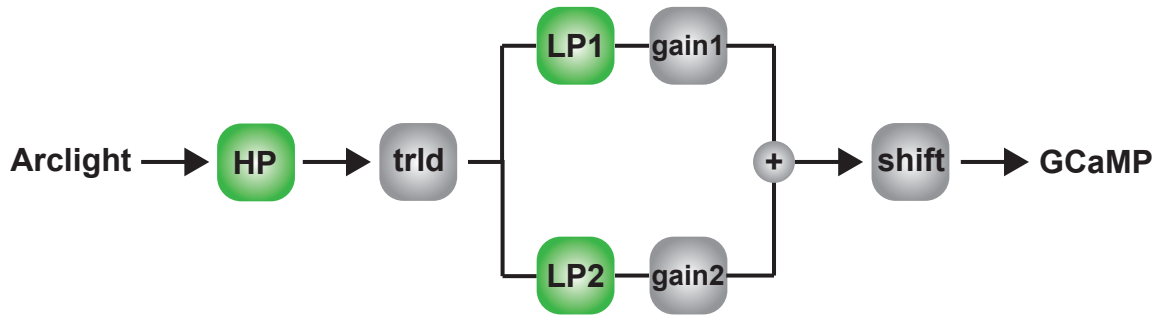


Figure 3. T4c direction tuning : (A) T4c Arclight (black) and GCaMP6f (red) normalized peak responses to grating moving in 12 directions at 4 different speeds. (n = 20 ROIs from N = 10 flies for Arclight, n = 18, N = 9 for GCaMP6f) (B) T4c Arclight (black) and GCaMP6f (red) normalized peak responses to grating moving in 12 directions at 4 different contrasts. (n = 23, N = 11 for Arclight, n = 22, N = 9 for GCaMP6f) (C) The directional tuning index L_{dir} for grating moving at 4 different speeds. The directional tuning index is calculated as the vector sum of the peak responses divided by the sum of all individual vector magnitudes. (D) The directional tuning index for grating at 4 different contrasts. All data shows the mean \pm SEM measured in 5 different flies.

A Simple Model



B Additive Model



C Multiplicative Model

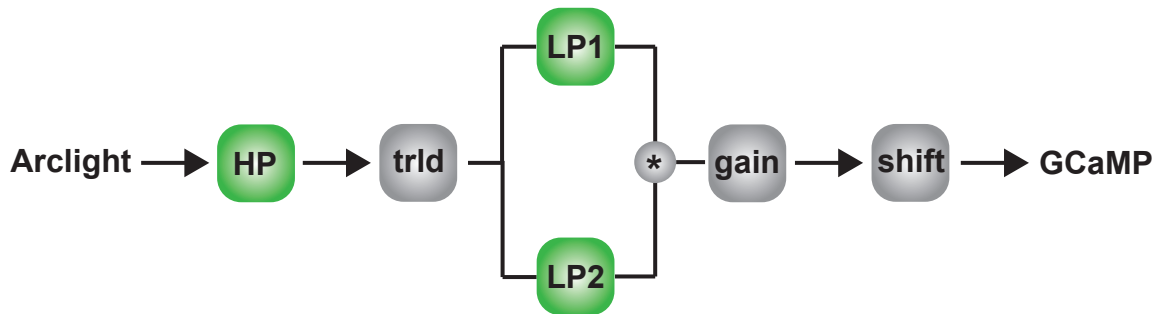


Figure 4. Models for voltage to calcium transformation : (A) Simple model consisting of High-Pass filter (HP), threshold (trld), Low-Pass filter (LP), gain and shift. (B) Additive model combining output of two low-pass filters via addition. (C) Multiplicative model combining output of two low-pass filters via multiplication.

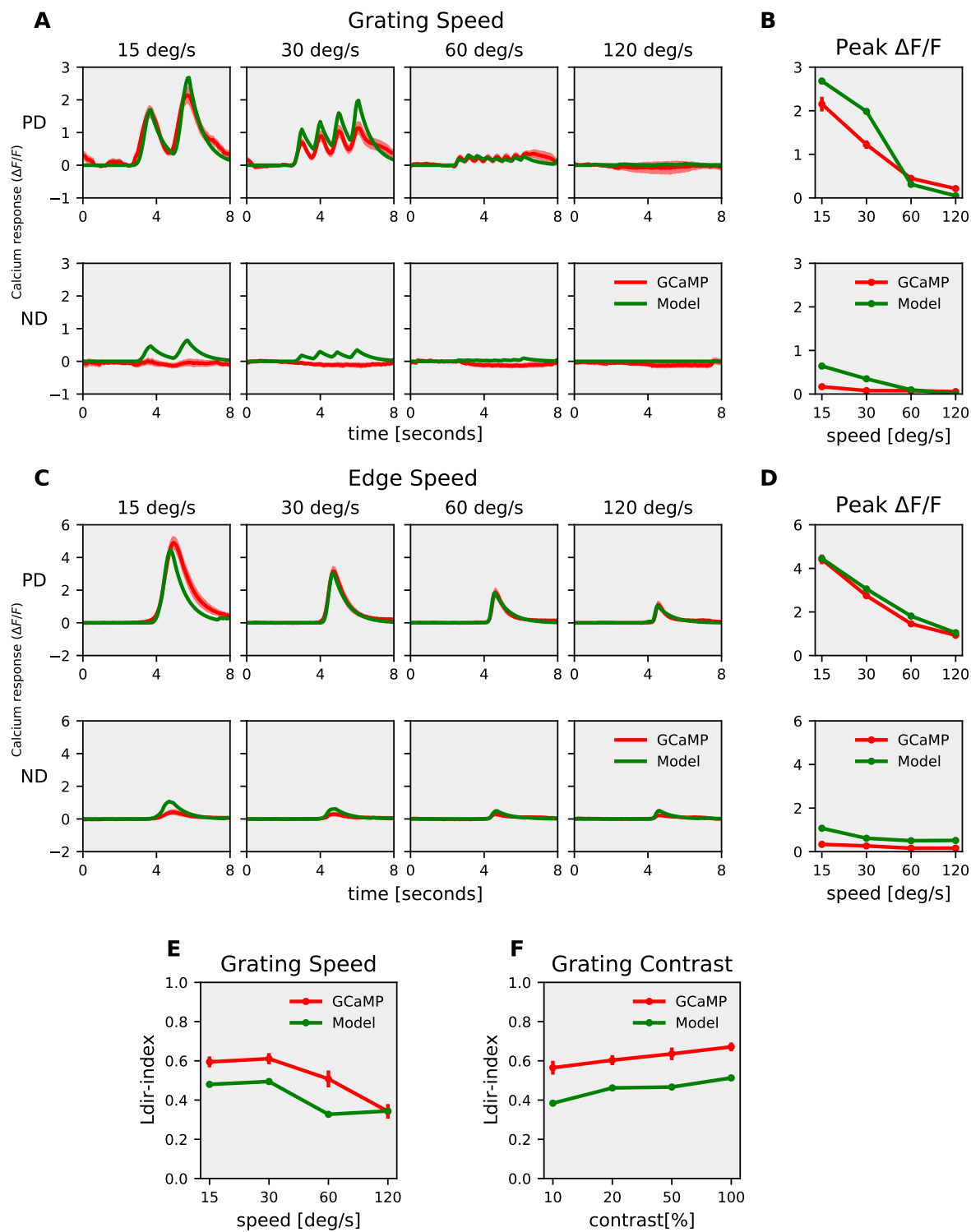


Figure 5. Multiplicative model responses : (A) T4c GCaMP6f (red) and multiplicative model (green) responses to grating moving in PD (top row) and ND (bottom row) at 4 different speeds. (B) T4c GCaMP6f and model peak responses to grating moving in PD (top) and ND (bottom) at 4 different speeds. (C) T4c GCaMP6f (red) and multiplicative model (green) responses to ON-edge moving in PD (top row) and ND (bottom row) at 4 different speeds. (D) T4c GCaMP6f and model peak responses to ON-edge moving in PD (top) and ND (bottom) at 4 different speeds. (E) The directional tuning index L_{dir} for GCaMP6f and model for grating moving in 12 directions at 4 different speeds. (F) The directional tuning index L_{dir} for GCaMP6f and model for grating moving in 12 directions at 4 different contrasts.

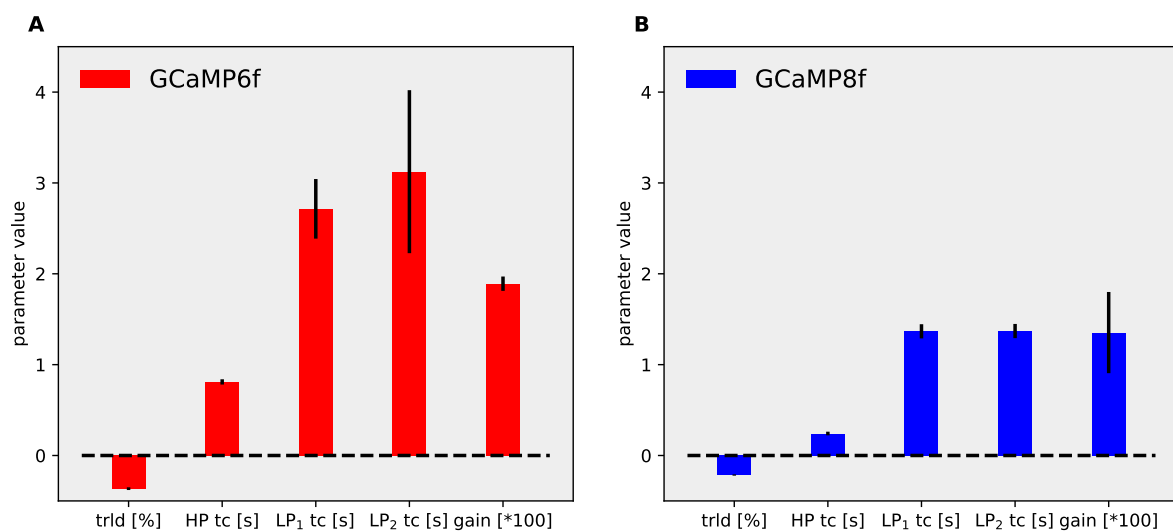


Figure 6. Model parameters for GCaMP6f (A) and GCaMP8f (B) : Data shows mean \pm SD for optimal parameters for the multiplicative model. The data were fit for grating moving in 12 directions and 4 speeds, and for ON-edge moving in PD and ND at 4 speeds. trld : threshold, HP : High Pass, LP : Low Pass, tc : Time constant

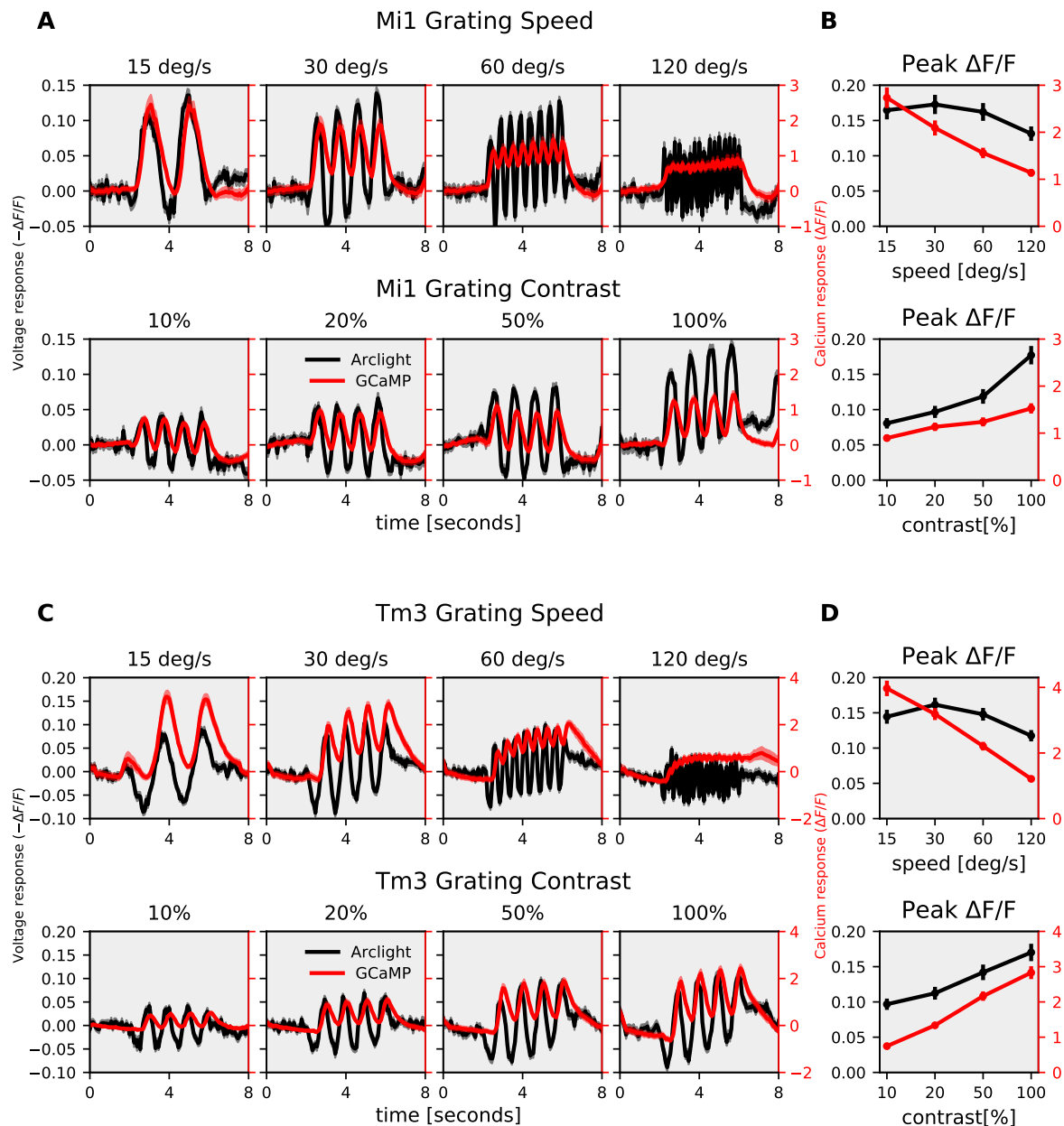


Figure 7. Mi1, Tm3 speed and contrast dependence : (A) Mi1 Arlight (black) and GCaMP6f (red) responses to grating moving at 4 different speeds (top row) and 4 different contrasts (bottom row). The plots have twin y-axis. The left y-axis of the plot represents voltage responses i.e. changes in Arlight fluorescence ($-\Delta F/F$) and the right y-axis of the plot represents calcium responses i.e. changes in GCaMP6f fluorescence ($\Delta F/F$) (B) Mi1 peak responses to grating moving at 4 different speeds ($n = 24$ ROIs from $N = 5$ flies for Arlight, $n = 19$, $N = 8$ for GCaMP) and 4 different contrasts ($n = 24$, $N = 5$ for Arlight, $n = 22$, $N = 8$ for GCaMP). (C) Tm3 Arlight (black) and GCaMP6f (red) responses to grating moving at 4 different speeds (top row) and 4 different contrasts (bottom row). (D) Tm3 peak responses to grating moving at 4 different speeds ($n = 52$, $N = 5$ for Arlight, $n = 37$, $N = 4$ for GCaMP) and 4 different contrasts ($n = 35$, $N = 5$ for Arlight, $n = 36$, $N = 4$ for GCaMP). All data shows the mean \pm SEM.

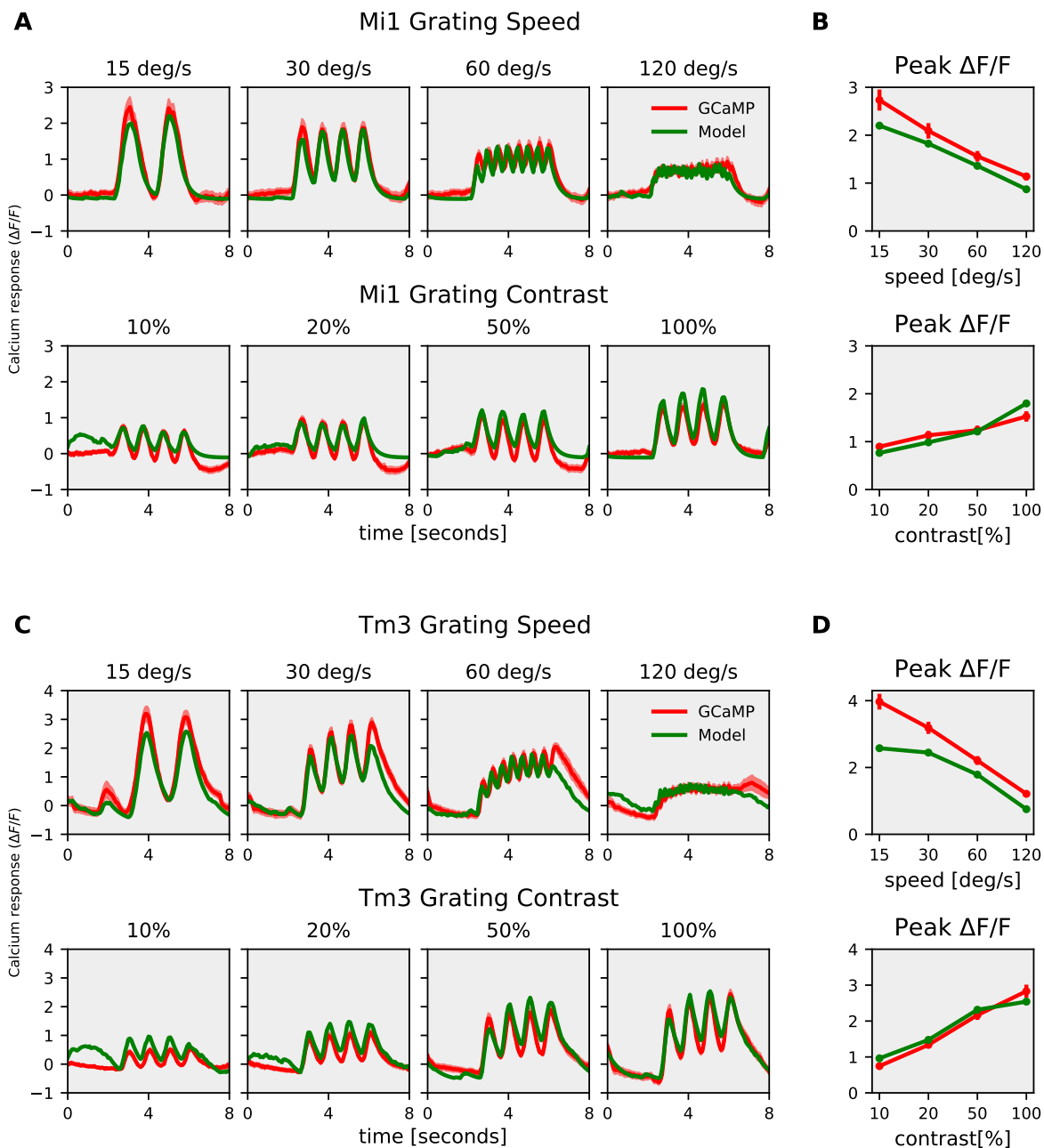


Figure 8. Mi1, Tm3 Simple model responses : (A) Mi1 GCaMP6f (red) and model (green) responses to gratings moving at 4 different speeds (top row) and to gratings moving at 4 different contrasts (bottom row). (B) Mi1 GCaMP6f and model peak responses to gratings moving at 4 different speeds (top) and 4 different contrasts (bottom). (C) Tm3 GCaMP6f (red) and model (green) responses to gratings moving at 4 different speeds (top row) and to gratings moving at 4 different contrasts (bottom row). (D) Tm3 GCaMP6f and model peak responses to gratings moving at 4 different speeds (top) and 4 different contrasts (bottom).

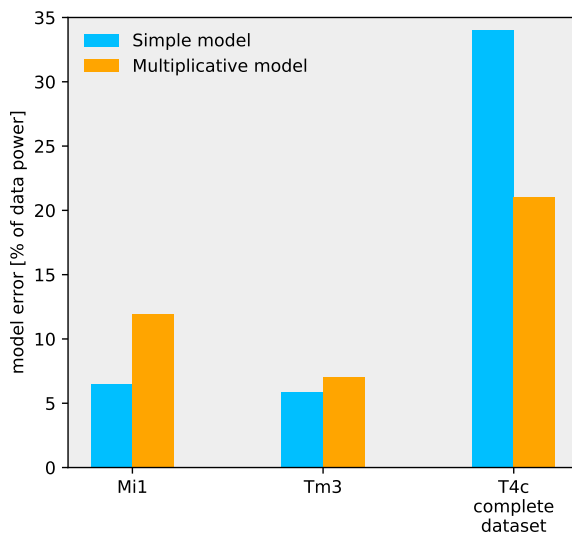


Figure 9. Model error for the simple and multiplicative model : The model error for the simple model (blue) and multiplicative model (orange). Mi1 and Tm3 dataset consists of gratings at 4 different speeds and contrast moving in a single direction. T4c complete dataset consists of gratings moving in 12 different directions, and ON edge moving in PD, ND at 4 different speeds and contrasts i.e. a total of 112 stimuli conditions.